

A complete parton level analysis of boson-boson scattering and ElectroWeak Symmetry Breaking in $\ell\nu$ + four jets production at the LHC.

Alessandro Ballestrero^a, Giuseppe Bevilacqua^c and Ezio Maina^{a,b}

^a *INFN, Sezione di Torino, Italy,*

^b *Dipartimento di Fisica Teorica, Università di Torino, Italy*

^c *Institute of Nuclear Physics, NCSR Demokritos, 15310 Athens, Greece.*

ABSTRACT: A complete parton level analysis of $\ell\nu$ + four jets production at the LHC is presented, including all processes at order $\mathcal{O}(\alpha_{EM}^6)$, $\mathcal{O}(\alpha_{EM}^4\alpha_S^2)$ and $\mathcal{O}(\alpha_{EM}^2\alpha_S^4)$. The infinite Higgs mass scenario, which is considered as a benchmark for strong scattering theories and is the limiting case for composite Higgs models, is confronted with the Standard Model light Higgs predictions in order to determine whether a composite Higgs signal can be detected as an excess of events in boson–boson scattering.

Contents

1. Introduction	1
2. Outline of the analysis	4
3. Calculation	6
4. Pure Electroweak processes	10
5. The VVjj QCD background	12
6. Full analysis	14
7. Dependence on the jet cone size	22
8. Conclusions	24

1. Introduction

The mechanism of Electro–Weak Symmetry Breaking (EWSB) will be a central issue in the physics program at the LHC¹. The Standard Model (SM) describes this phenomenon in an extremely simple and economical fashion through the Higgs mechanism. The fit of EW precision data is in agreement with the SM predictions to an unprecedented accuracy and gives an upper limit on the Higgs mass of about 182 GeV [6], while direct searches imply $m_H > 114$ GeV [7]. Any attempt to go beyond the SM is severely constrained and made difficult by the very success the SM has achieved.

The first question to which the LHC must provide an answer is whether or not a light Higgs exists. If the Higgs is not found then the SM and its most promising extension, the MSSM, will be ruled out.

In this case scattering processes between longitudinally polarized vector bosons will play a prominent role because, without a Higgs, the corresponding amplitudes grow with energy and violate perturbative unitarity at about one TeV [8]. However, since unitarity is essentially the statement of conservation of total probability it cannot be violated in Nature and some new phenomena must intervene at an energy scale within reach for the LHC.

Many alternative mechanisms of EWSB have been explored. For instance EWSB may result from strong dynamics in a hitherto undiscovered sector, as postulated by Technicolor

¹Detailed reviews and extensive bibliographies can be found in Refs.[1, 2, 3, 4, 5]

theories. Alternatively, EWSB may be a consequence of boundary conditions satisfied by gauge fields in compactified additional space dimensions. In this case, new states, the tower of Kaluza–Klein modes generated by expanding the fields along the compactified directions, would tame the growth of Vector–Vector (VV) scattering. However, typically, Technicolor and Higgsless theories have difficulties with EW precision data and with the generation of fermion masses.

A more pragmatical approach is based on the language of the Effective Electro–Weak Lagrangian [9], in which the SM is interpreted as the first term in an expansion in E/Λ of an unknown high energy theory characterized by a mass scale Λ which acts as a cut–off compared with the energy E at which the theory is probed, or equivalently on the anomalous couplings [10] description. This strategy can be supplemented by the adoption of one of the many schemes for turning perturbative scattering amplitudes into amplitudes which satisfy by construction the unitarity constraints. This procedure, in analogy with low energy QCD, which can be expressed by exactly the same formalism which describes the Higgs sector in the SM, leads to expect the presence of resonances in VV scattering. Unfortunately the mass, spin and even number of these resonances are not uniquely determined [11, 12, 13] from theory. Again, a detailed study of the two–boson mass distribution in VV scattering will be mandatory in order to clarify the details of the resulting spectrum.

The discovery of one or more Higgs particle(s) will trigger the effort to measure its properties as accurately as possible, beginning with its mass and its coupling to the other particles. It should be noted that the Goldstone theorem and the Higgs mechanism do not require the existence of elementary scalars. It is conceivable and widely discussed in the literature that composite states are responsible for EWSB as nicely recently reviewed in Ref. [14]. For instance in [15] the Higgs is identified with a pseudoGoldstone boson, while more recently additional possibilities have been explored: the Little Higgs [16], the gauge–Higgs unification [17, 18] and the holographic Higgs [19]. These theories are characterized by the presence of new states which could be produced at the LHC, if light enough. In view of the large number of different proposals it is useful to determine the model independent features of this class of theories. There has been recent progress in this area [20, 21, 22], using the effective theory language. The leading effects are described by two parameters (one for a universal modification of all Higgs couplings, and the other one for a universal modification of Higgs couplings to fermions) characterized by the ratio v^2/f^2 , where v is the Higgs vacuum expectation value and f is the σ –model scale. Again, a test of Higgs compositeness at the LHC requires an analysis of longitudinal gauge–boson scattering. Indeed, because of the modified Higgs couplings, longitudinal gauge–boson scattering amplitudes violate unitarity at high energy, even in the presence of a light Higgs [21]. The E^2 –growing amplitude is a factor v^2/f^2 smaller than in the Higgsless case and the violation is moved to a larger energy regime. As a consequence, the scattering cross section for an infinitely massive Higgs in the SM represents, at large energies, an upper limit for VV scattering processes in this class of theories, and can be taken as a benchmark for the observability of signals of strong scattering and of Higgs compositeness in boson–boson reactions. It should be mentioned that in any case the rise of the cross section at large invariant VV mass will be masked by the decrease of the parton luminosities at large momentum fractions and, as

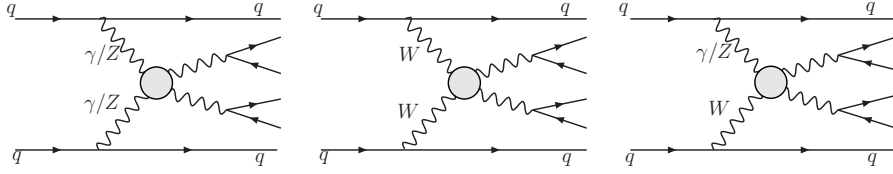


Figure 1: Vector boson fusion processes

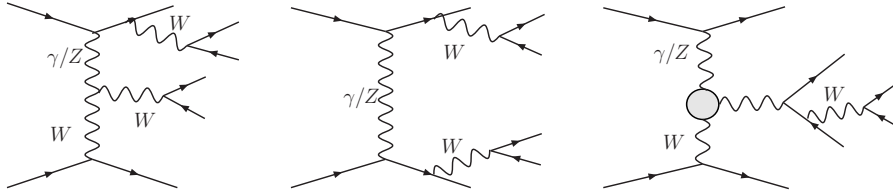


Figure 2: Non fusion and non doubly resonant two vector boson production.

a consequence, will be particularly challenging to detect.

Therefore, even if a light Higgs is discovered, boson–boson scattering is a crucial process to study, which can give us useful information on the nature of the Higgs boson. It is worth pointing out that, in this framework, since the Higgs can be viewed as an approximate fourth Goldstone boson, its properties are related to those of the exact (eaten) Goldstone bosons. Strong gauge-boson scattering will be accompanied by strong Higgs pair production [21].

Scattering processes among vector bosons have been scrutinized since a long time [23, 24]. In most cases previous studies of boson–boson scattering at high energy hadron colliders have resorted to some approximation, either the Equivalent Vector Boson Approximation (EVBA) [25], or a production times decay approach. In Ref. [26, 27] an analysis of $l\nu + \text{four jets}$ and $\mu^+\mu^- + \text{four jets}$ production at the LHC has been presented, with the limitation of taking into account only purely electroweak processes. Preliminary results concerning the inclusion of the $\mathcal{O}(\alpha_{EM}^4 \alpha_S^2)$ background, which include $VV + 2j$ and top–antitop production have appeared in Ref. [28]. In the last few years QCD corrections to boson–boson production via vector boson fusion [29] at the LHC have been computed and turn out to be below 10%. While the present paper was being finalized, VBFNLO [30] a Monte Carlo program for vector boson fusion, double and triple vector boson production at NLO QCD accuracy, limited to the leptonic decays of vector bosons, has been released

In this paper we study at parton level the process $pp \rightarrow l\nu + 4j$, including all backgrounds contributing to this six parton final state. We use complete tree level matrix elements. We consider two scenarios: a light Higgs SM framework with $M_H = 200$ GeV and an infinite mass Higgs scenario. The production cross section for $l\nu + 4j$ has been shown to be much larger [26, 27] than that for $\mu^+\mu^- + 4j$ making it the most promising candidate for boson–boson scattering studies provided the full QCD background can be kept under control. Processes in which both vector bosons decay leptonically suffer from a

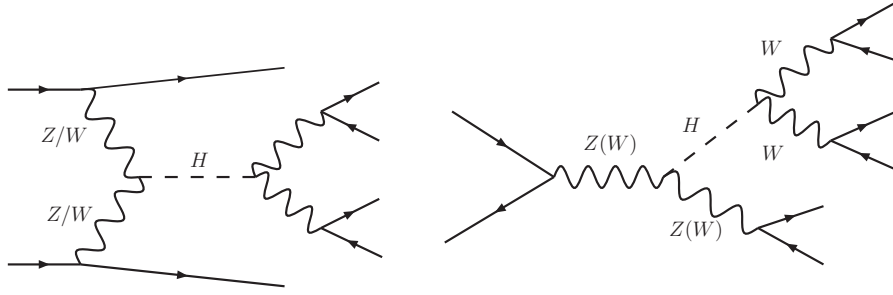


Figure 3: Higgs boson production via vector boson fusion and Higgsstrahlung.

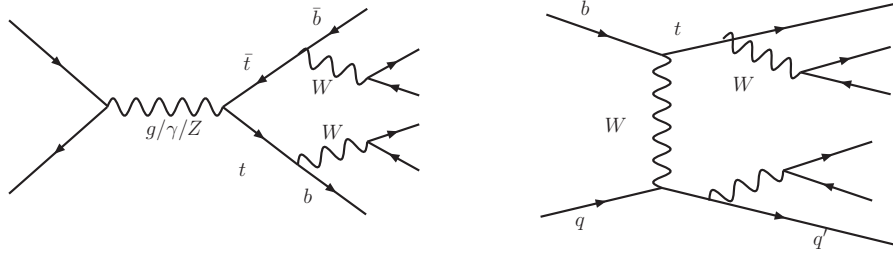


Figure 4: Electroweak $t\bar{t}$ and single top production.

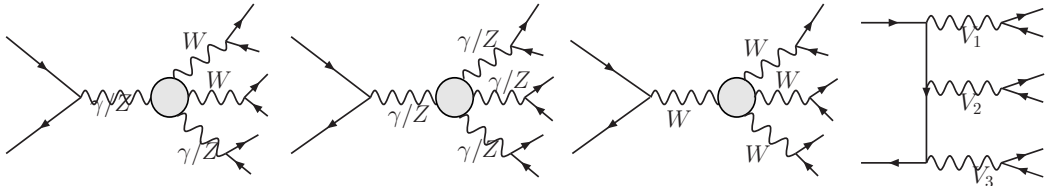


Figure 5: Three vector boson production.

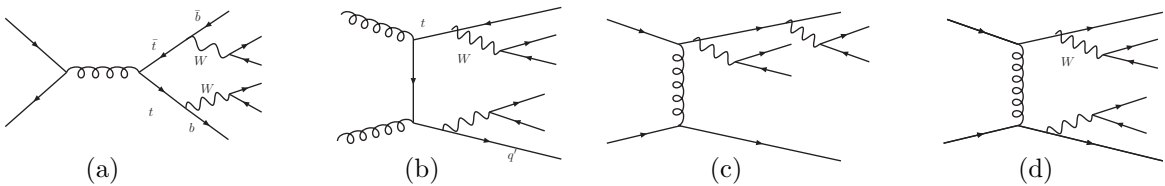


Figure 6: Examples of contributions to the QCD irreducible background: $t\bar{t}$ production (a,b) and $VV + 2j$ (c,d)

much smaller rate despite a reduced QCD background.

2. Outline of the analysis

The observation of strong boson–boson scattering as an excess of events compared to the SM prediction requires, as an essential condition, that a signal of VV scattering is extracted

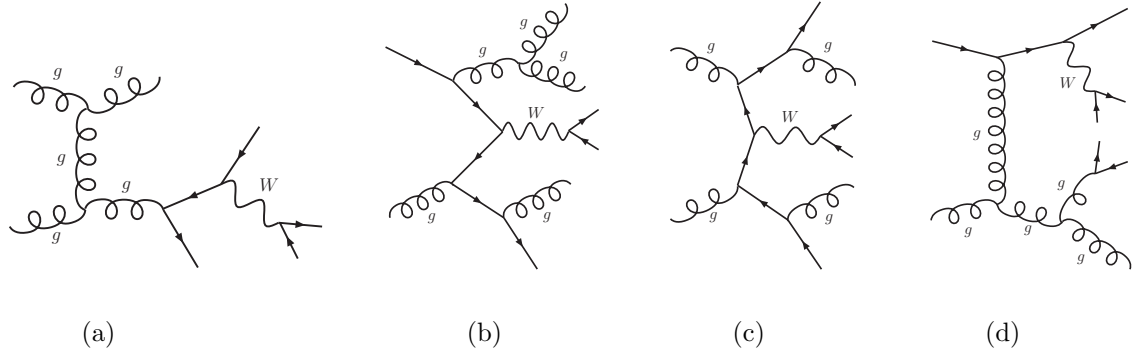


Figure 7:

Representative Feynman diagrams for the $\mathcal{O}(\alpha_{EM}^2 \alpha_S^4)$, $W + 4j$ production processes at the LHC.

from the background. At the same time the selection strategy must be capable to maximize the differences between the light Higgs and the no-Higgs cases. Three perturbative orders contribute to the background. At $\mathcal{O}(\alpha_{EM}^6)$ there are a large number of diagrams which cannot be interpreted as boson-boson scattering and which cannot be separated in any sensible way from the scattering type diagrams due to large cancellations between the two sets [27]. At $\mathcal{O}(\alpha_{EM}^4 \alpha_S^2)$ we have to deal with the production of two electroweak bosons plus two jets without any scattering contribution. At $\mathcal{O}(\alpha_{EM}^2 \alpha_S^4)$ only one electroweak boson is effectively produced, while the additional jets, which do not peak at any particular mass, populate the full available phase space with a production rate which is much larger than the signal one.

In this section we briefly describe how the analysis on $\ell\nu + 4j$ final states has been performed. Basically, the whole procedure can be summarized in three steps:

- apply a set of kinematical cuts to isolate a sample of candidate scattering events;
- define a Vector Boson Scattering (VBS) signal on this enriched sample;
- develop a statistical treatment of the signal to estimate the probability of observing an excess in terms of confidence levels.

The first step is concerned with the identification of a suitable kinematical signature which allows to capture the essence of VV scattering. The selection of events widely separated in pseudorapidity is a well established technique for enhancing the scattering contributions at LHC [23, 24]. Looking at the topology of the diagrams embedding the gauge boson scattering as a subprocess in Fig. 1, one concludes that it is appropriate to associate the two most forward/backward jets to the tag quarks which radiate the bosons which initiate VV scattering and to relate the two most central jets to the hadronic decay of a W or a Z in the final state. The main purpose of this kinematical selection is to isolate a sample of genuine $VV + 2j$ events while suppressing the contribution of irreducible backgrounds such as three boson production or top quark production, either from single top or top-antitop pairs. Additional cuts have been imposed in order to discriminate more effectively between

the light Higgs and the no Higgs scenarios. Unfortunately, this procedure does not fully screen from the QCD background entering $VV + 2j$ and additional, *ad hoc*, cuts must be applied to this purpose.

Having isolated a sample of candidate scattering events, one needs to define an observable quantity which is as susceptible as possible to the details of the mechanism of EWSB in order to maximize the sensitivity to effects of alternative models such as strong scattering. This task is straightforward only apparently. As already mentioned, a number of fake hits is expected to come from the QCD background, mainly in the form of $W + 4j$, as a consequence of the large cross section and gluon combinatorics which characterize this kind of contributions. The classical approach is to focus on the invariant mass distribution of the final state boson pair. The large QCD background, with its large scale uncertainty, makes this procedure rather dubious. A possible way out for this problem is to look instead at the invariant mass of the two central jets ($M_{j_c j_c}$) for events with large vector pair mass.

Provided a convenient set of kinematical cuts has been applied, the $\mathcal{O}(\alpha_{EM}^6) + \mathcal{O}(\alpha_{EM}^4 \alpha_S^2)$ cross section is dominated by the W and Z peaks, while the $\mathcal{O}(\alpha_{EM}^2 \alpha_S^4)$ ($W + 4j$) contribution is non-resonant in this respect. When restricting to the window between 70 and 100 GeV, which covers completely the W and Z resonances, we find that the $W + 4j$ distribution is essentially flat and therefore can reliably be measured from the sidebands of the physical region of interest. This procedure has two advantages. On one side, it drastically reduces the theoretical uncertainty associated to the scale dependence of the cross section, which mainly affects the $\mathcal{O}(\alpha_{EM}^2 \alpha_S^4)$ contribution. On the other side, it allows to subtract the dominant contribution to the irreducible QCD background, thus enhancing the visibility of genuine EWSB effects.

Once the non-resonant background has been subtracted, one is left with a peak whose size is strictly related to the regime of the EWSB dynamics: a strongly-coupled scenario would result in a more prominent peak than a weakly-coupled one. This feature suggests to take the integral of the peak as the discriminator among different models. At a given collider luminosity, the number of expected events can be derived. With a slight abuse of language, we call this number the VBS signal. It is by analyzing the probability density function (p.d.f.) associated with this discriminator that we can determine, in the last step, the confidence level for a given experimental result to be or not to be SM-like, in the same spirit of the statistical procedure adopted for the search of the Standard Model Higgs boson at LEP [31].

3. Calculation

As discussed in Sect. 2, three perturbative orders contribute to $\ell\nu + 4j$ at the LHC.

The $\mathcal{O}(\alpha_{EM}^6)$ and $\mathcal{O}(\alpha_{EM}^4 \alpha_S^2)$ samples have been generated with PHANTOM [33, 34, 35], while the $\mathcal{O}(\alpha_{EM}^2 \alpha_S^4)$ sample has been produced with MADEVENT [36]. Both programs generate events in the Les Houches Accord File Format [37]. In all samples full $2 \rightarrow 6$ matrix elements, without any production times decay approximation, have been used. The cuts in Tab. 1 have been applied at generation level.

Generation cuts
$p_T(\ell^\pm) > 20 \text{ GeV}$
$ \eta(\ell^\pm) < 3.0$
$p_T(j) > 30 \text{ GeV}$
$ \eta(j) < 6.5$
$M(jj) > 60 \text{ GeV}$

Table 1: Standard acceptance cuts applied in the event generation and present in all results. Here $j = d, u, s, c, b, g$: any pair of colored partons must have mass larger than 60 GeV.

For the Standard Model parameters we use the input values:

$$\begin{aligned}
M_W &= 80.40, & M_Z &= 91.187 \text{ GeV}, \\
G_\mu &= 1.16639 \cdot 10^{-5} \text{ GeV}^{-2}, & \alpha_s(M_Z) &= 0.118 \\
M_t &= 175.0 \text{ GeV}, & M_b &= 4.8 \text{ GeV}.
\end{aligned} \tag{3.1}$$

The masses of all other partons have been set to zero. We adopt the standard G_μ -scheme to compute the remaining parameters.

All samples have been generated using CTEQ5L [38] parton distribution functions. For the $\mathcal{O}(\alpha_{EM}^6)$ and $\mathcal{O}(\alpha_{EM}^4 \alpha_S^2)$ samples, generated with PHANTOM, the QCD scale has been taken as:

$$Q^2 = M_W^2 + \frac{1}{6} \sum_{i=1}^6 p_{Ti}^2 \tag{3.2}$$

while for the $\mathcal{O}(\alpha_{EM}^2 \alpha_S^4)$ sample the scale has been set to $Q^2 = M_Z^2$. This difference in the scales conservatively leads to a definite relative enhancement of the $W + 4j$ background. Tests in comparable reactions at $\mathcal{O}(\alpha_{EM}^2 \alpha_S^4)$ have shown an increase of about a factor of 1.5 for the processes computed at $Q^2 = M_Z^2$ with respect to the same processes computed with the larger scale Eq.(3.2).

We work at parton level with no showering and hadronization. The two jets with the largest and smallest rapidity are identified as forward and backward tag jet respectively. The two intermediate jets are considered as candidate vector boson decay products.

The neutrino momentum is reconstructed according to the usual prescription, requiring the invariant mass of the $\ell\nu$ pair to be equal to the W boson nominal mass,

$$(p^\ell + p^\nu)^2 = M_W^2, \tag{3.3}$$

in order to determine the longitudinal component of the neutrino momentum. This equation has two solutions,

$$p_z^\nu = \frac{\alpha p_z^\ell \pm \sqrt{\alpha^2 p_z^{\ell 2} - (E^{\ell 2} - p_z^{\ell 2})(E^{\ell 2} p_T^{\nu 2} - \alpha^2)}}{E^{\ell 2} - p_z^{\ell 2}}, \tag{3.4}$$

where

$$\alpha = \frac{M_W^2}{2} + p_x^\ell p_x^\nu + p_y^\ell p_y^\nu. \tag{3.5}$$

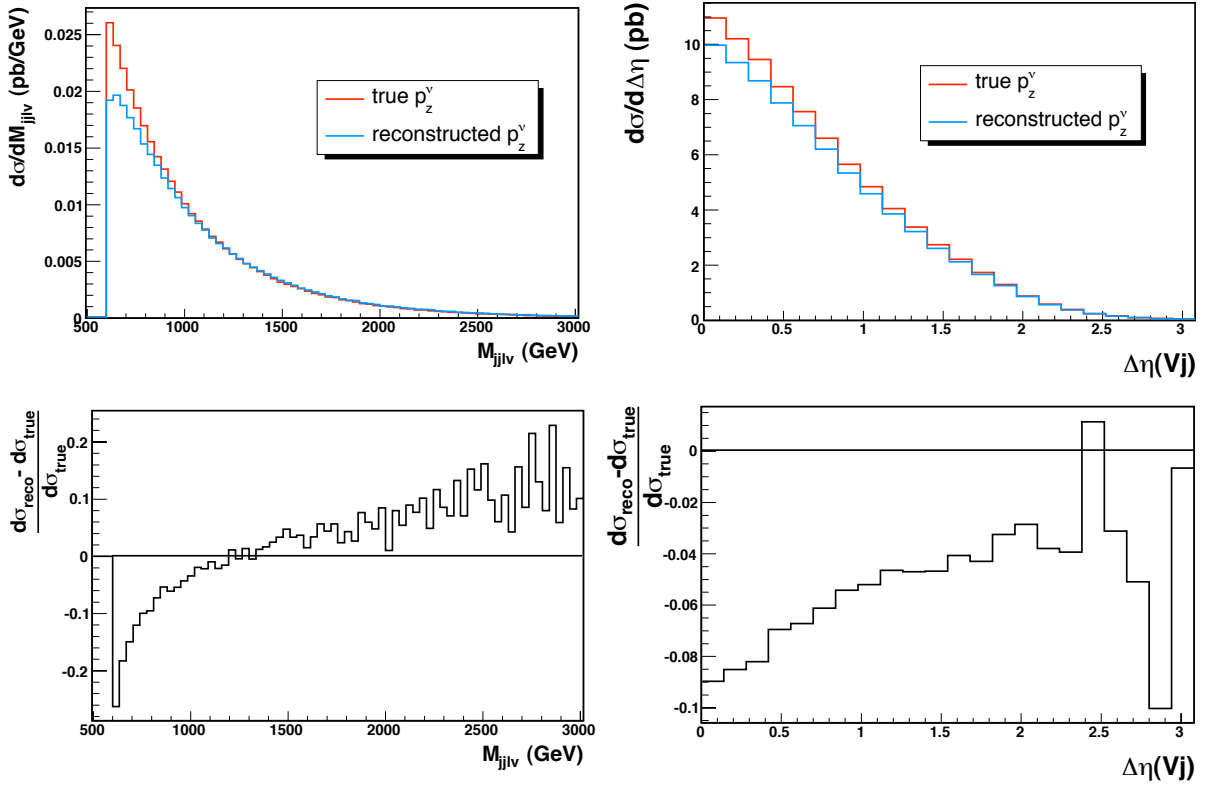


Figure 8: Distribution of the invariant mass $M(j_c j_c \ell \nu)$ (left hand side) and of the minimum $\Delta\eta$ between any reconstructed heavy boson and any tag jet (right hand side). The red line is obtained using the actual longitudinal momentum of the neutrino while the blue line is obtained using the reconstructed value. The lower row plots present the relative difference between the two results. Cuts as listed in Tab. 1, with the addition of $|\Delta\eta(j_f j_b)| > 3.8$ and $M_{j_c j_c \ell \pm \nu} > 600$ GeV. The numbers refer to the $\mu\nu + 4j$ channel only.

If the discriminant of Eq.(3.4) is negative, which happens only if the actual momenta satisfy $(p^\ell + p^\nu)^2 > M_W^2$, it is reset to zero. The corresponding value of p_z^ν is adopted. This value of p_z^ν results in the smallest possible value for the mass of the $\ell\nu$ pair which is compatible with the measured components of p^ℓ and p^ν . The corresponding mass is always larger than M_W . If the determinant is positive and the two solutions for p_z^ν have opposite sign we choose the solution whose sign coincides with that of p_z^ℓ . If they have the same sign we choose the solution with the smallest $\Delta R = \sqrt{\Delta\eta^2 + \Delta\phi^2}$ with the charged lepton. The reconstructed value is used for computing all physical observables.

The reconstruction procedure detailed above is commonly used by the experimental collaborations, see for instance Ref. [39]. While unavoidable, any neutrino reconstruction necessarily modifies the actual event kinematics and introduces some uncertainty in the measurement. It should be noticed, however, that systematic biases introduced by the reconstruction algorithm, once identified through the analysis of Monte Carlo events, can be corrected for when analyzing actual data. In order to estimate the effect of the neutrino

reconstruction on our results, in Fig. 8 we show the distribution of the invariant mass $M(j_c j_c l \nu)$ (left hand side) and of the minimum $\Delta\eta$ between any reconstructed heavy boson and any tag jet (right hand side). These two quantities are the main kinematical variables which depend on the reconstructed neutrino longitudinal momentum and which will be used in the analysis. The remaining one is $M(j l \nu)$ which enters the antitop selection and which normally affects events close to the top pair production threshold, which is sizably smaller than the typical energy scale at which VV scattering is studied.

The total cross section is about 10% larger with actual neutrino momenta than with the reconstructed ones. The difference is concentrated at small $M(j_c j_c l \nu)$ masses and small $\Delta\eta$ separations. Since in the following we are going to focus on the region of large invariant masses and we are going to require a minimum separation between any reconstructed heavy boson and any tag jet, $|\Delta\eta(Vj)| > 0.6$, the reconstruction effects are modest. We are mainly concerned with the comparison of the light Higgs and the no-Higgs scenarios which are affected in the same way by the neutrino reconstruction. Moreover, we are in any case forced to consider measurable quantities, which can only be defined through reconstructed variables.

Basic selection cuts
$70 \text{ GeV} < M(j_c j_c) < 100 \text{ GeV}$
$M(j_f j_b) < 70 \text{ GeV}; M(j_f j_b) > 100 \text{ GeV}$
$ M(j j j; j \ell^\pm \nu_{rec}) - M_{top} > 15 \text{ GeV}$
$\Delta R(j j) > 0.3$

Table 2: These cuts have been adopted in order to separate Boson Fusion from $t\bar{t}$ and single-top production and from three-vector-boson production.

For very large Higgs masses, all Born diagrams with Higgs propagators become completely negligible in the Unitary Gauge we work in and the expectations for all processes reduce to those in the $M_H \rightarrow \infty$ limit.

On the generated samples we have applied some basic selection cuts. There are a number of backgrounds which can be distinguished from the Boson Fusion signal because of the mass distribution of their final states. They are $t\bar{t}$ and single-top production (see Fig. 4 and the left half of Fig. 6) and three-vector-boson production (see Fig. 5). For this purpose, we have required that no jet triplet satisfies

$$|M_{jjj} - M_t| < 15 \text{ GeV} \quad (3.6)$$

and no jet satisfies

$$|M_{jl\nu} - M_t| < 15 \text{ GeV}. \quad (3.7)$$

The invariant mass of the two central jets is required to be compatible with the decay of an electroweak boson,

$$70 \text{ GeV} < M(j_c j_c) < 100 \text{ GeV}. \quad (3.8)$$

Moreover we have required the mass of the forward and backward jet pair to lie outside the mass window of the electroweak bosons in order to exclude three-vector-boson production.

At large transverse momentum, jet pairs with mass comparable to the mass of electroweak bosons or even larger can merge into one single jet when an angular measure like $\Delta R(jj)$ is adopted for reconstructing jets. Therefore we have imposed that all partons satisfy $\Delta R(jj) > 0.3$. In Sect. 7 we discuss in more detail the effect of removing the angular separation constraint or, on the contrary, of imposing a more stringent requirement $\Delta R(jj) > 0.5$. For later convenience these further cuts are summarized in Tab. 2

4. Pure Electroweak processes

In this section, as a preliminary step, we compare in some detail the $\mathcal{O}(\alpha_{EM}^6)$ sample with a 200 GeV Higgs with the corresponding sample with the Higgs mass taken to infinity, using a simplified set of cuts compared to Ref. [26]. In Ref. [26] the analysis was primarily based on a neural network approach. Here we prefer to apply a set of physically transparent cuts which can be generalized to the complete analysis. The distributions in [26] clearly show that, at large invariant masses of the boson–boson pair, the exact value of the Higgs mass is irrelevant, provided it is sizably smaller than the boson–boson mass range under investigation. Therefore the case of a 200 GeV mass discussed in this paper is representative of the full light Higgs mass range up to a few hundreds GeV.

M_{cut}	no Higgs		$M_H = 200$ GeV		ratio
	σ	events	σ	events	
400 GeV	19.875 fb	1988	18.254 fb	1825	1.09
600 GeV	9.803 fb	980	7.951 fb	795	1.23
800 GeV	4.910 fb	491	3.848 fb	385	1.28
1000 GeV	2.624 fb	262	2.075 fb	208	1.26
1200 GeV	1.413 fb	141	1.132 fb	113	1.25
1400 GeV	0.753 fb	75	0.614 fb	61	1.23
1600 GeV	0.377 fb	38	0.374 fb	37	1.03

Table 3: Integrated $\mathcal{O}(\alpha_{EM}^6)$ cross section for $M(j_c j_c l \nu) > M_{cut}$ and number of expected events after one year at high luminosity ($\mathcal{L} = 100 \text{ fb}^{-1}$) with the set of cuts listed in Tabs. 1, 2. The numbers refer to the $\mu\nu + 4j$ channel only.

We start presenting in Tab. 3 the integrated cross section for $M(j_c j_c l \nu) > M_{cut}$ and the number of expected events after one year at high luminosity ($\mathcal{L} = 100 \text{ fb}^{-1}$) for several M_{cut} values. These results have been obtained with the set of cuts listed in Tabs. 1, 2 and refer to a single lepton family. Taking $M_{cut} = 1000$ GeV as an example we have a SM prediction of about 200 events per year and an excess of about 50 events in the no Higgs case.

The distribution of the mass of the charged lepton, (reconstructed) neutrino and the two most central jets is shown on the left hand side of Fig. 9. The separation between the two cases, which we estimate from the ratio of the expected number of signal events in the two scenarios, can be increased imposing a large separation between the tag jets, which eliminates most of the non-scattering background, and requiring the reconstructed W which

Selection cuts
$ \Delta\eta(j_f j_b) > 4.0$
$ \eta(\ell\nu) < 2.0$

Table 4: Selection cuts applied in the analysis of the purely electroweak sample in addition to the basic cuts in Tabs. 1, 2

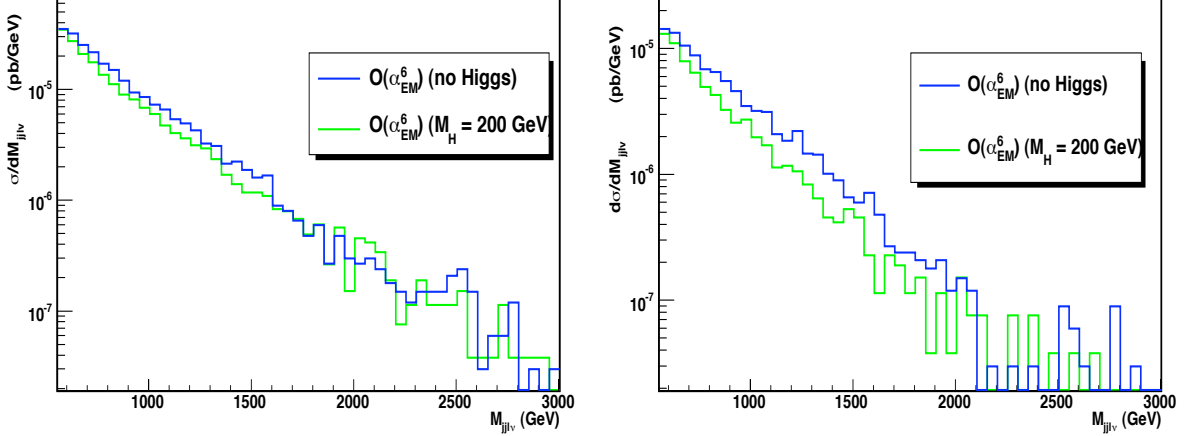


Figure 9: Invariant mass $M(j_c j_c l \nu)$ with the set of cuts listed in Tabs. 1–2 on the left hand side and with the addition of the cuts in Tab. 4 on the right hand side. The numbers refer to the $\mu\nu + 4j$ channel only.

M_{cut}	no Higgs		$M_H = 200$ GeV		ratio
	σ	events	σ	events	
400 GeV	8.327 fb	833	6.511 fb	651	1.28
600 GeV	4.138 fb	414	2.829 fb	283	1.46
800 GeV	2.129 fb	213	1.272 fb	127	1.68
1000 GeV	1.111 fb	111	0.626 fb	63	1.76
1200 GeV	0.594 fb	59	0.316 fb	32	1.84
1400 GeV	0.283 fb	28	0.159 fb	16	1.75
1600 GeV	0.137 fb	14	0.079 fb	8	1.75

Table 5: Integrated $\mathcal{O}(\alpha_{EM}^6)$ cross section for $M(j_c j_c l \nu) > M_{cut}$ and number of expected events after one year at high luminosity ($\mathcal{L} = 100 \text{ fb}^{-1}$) with the set of cuts listed in Tabs. 1–2 and 4. The numbers refer to the $\mu\nu + 4j$ channel only.

decays leptonically to be rather central, since the vector bosons tend to be produced more centrally in the absence of the Higgs boson. The applied cuts are summarized in Tab. 4 and the corresponding cross sections as a function of M_{cut} are presented in Tab. 5. The distribution of the VV mass is shown on the right hand side of Fig. 9. The improvement

in the separation of the two curves is clearly visible.

5. The VVjj QCD background

The $\mathcal{O}(\alpha_{EM}^4 \alpha_S^2)$ background is large. With the basic generation cuts in Tab. 1 it is about one hundred times larger than the $\mathcal{O}(\alpha_{EM}^6)$ contribution and it is dominated by $t\bar{t}$ and single-top production. Once the top-veto in Tab. 2 is imposed this background is severely reduced.

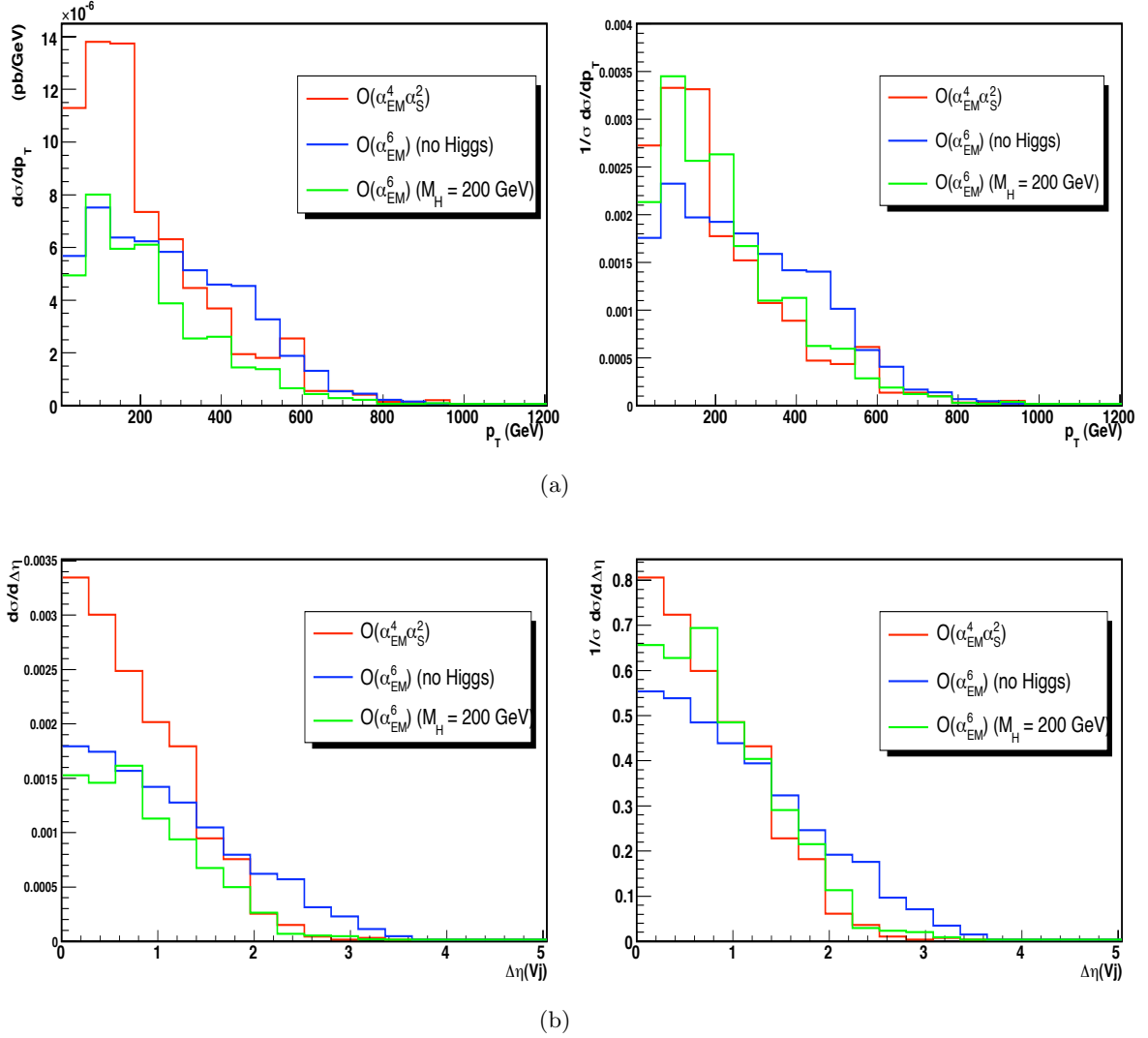


Figure 10: *Top:* distribution of the transverse momentum of the W reconstructed from leptons. *Bottom:* minimum $\Delta\eta$ between any reconstructed heavy boson and any tag jet. Cuts as listed in Tabs. 1–2, with the addition of $|\Delta\eta(j_f j_b)| > 4.0$. The plots on the right are the analogous of the ones on the left, but normalized to one. The numbers refer to the $\mu\nu + 4j$ channel only and to the region $M(j_c j_c l\nu) > 800\text{GeV}$

Selection cuts I
$ \Delta\eta(j_f j_b) > 4.0$
$p_T(\ell\nu) > 200 \text{ GeV}$
$ \Delta\eta(Vj) > 0.6$

Table 6: Selection cuts applied in the analysis of the $\mathcal{O}(\alpha_{EM}^6)$ and $\mathcal{O}(\alpha_{EM}^4\alpha_S^2)$ samples in addition to the cuts in Tabs. 1, 2.

Even in the absence of $W + 4j$ contributions, the previous selection procedure does not ensure a good separation between typical expectations from the Standard Model with a light Higgs and the benchmark no Higgs scenario. This is essentially due to the fact that the contribution of the QCD diagrams with a gluon exchanged in the t channel, Fig.6(c,d), is not substantially affected. However, a preliminary study at $\mathcal{O}(\alpha_{EM}^6) + \mathcal{O}(\alpha_{EM}^4\alpha_S^2)$ has devised a collection of observables which appear sensitive to the different kinematics of this kind of background[28, 27]. More specifically, it has been found that the transverse momentum of the reconstructed $\ell\nu$ pair and the angular separation between tag jets and the final state bosons are suitable signal-to-background discriminators. It was also realized that, in the presence of the $\mathcal{O}(\alpha_{EM}^4\alpha_S^2)$ background, requiring a large transverse momentum of the reconstructed $\ell\nu$ pair is more effective than the centrality requirement used previously. The distributions for $p_T(\ell\nu)$ and $|\Delta\eta(Vj)|$ are shown in Fig. 10.

M_{cut}	no Higgs		$M_H = 200 \text{ GeV}$		ratio
	σ	events	σ	events	
600 GeV	4.530 (2.640) fb	453 (264)	3.500 (1.427) fb	350 (143)	1.29 (1.85)
800 GeV	2.584 (1.553) fb	258 (155)	1.763 (0.754) fb	176 (75)	1.47 (2.07)
1000 GeV	1.354 (0.861) fb	135 (86)	0.881 (0.404) fb	88 (40)	1.53 (2.15)
1200 GeV	0.750 (0.478) fb	75 (48)	0.499 (0.219) fb	50 (22)	1.50 (2.18)
1400 GeV	0.357 (0.228) fb	36 (23)	0.270 (0.132) fb	27 (13)	1.33 (1.77)
1600 GeV	0.203 (0.124) fb	20 (12)	0.186 (0.077) fb	19 (8)	1.05 (1.50)

Table 7: Integrated $\mathcal{O}(\alpha_{EM}^6) + \mathcal{O}(\alpha_{EM}^4\alpha_S^2)$ cross section for $M(j_c j_c \ell\nu) > M_{cut}$ and number of expected events after one year at high luminosity ($\mathcal{L} = 100 \text{ fb}^{-1}$) with the set of cuts listed in Tabs. 1, 2 and Tab. 6. In parentheses the results for the $\mathcal{O}(\alpha_{EM}^6)$ contribution alone is also given. Interferences between the different perturbative orders are neglected. The numbers refer to the $\mu\nu + 4j$ channel only.

The integrated cross section for $M(j_c j_c \ell\nu) > M_{cut}$ and number of expected events after one year at high luminosity ($\mathcal{L} = 100 \text{ fb}^{-1}$) for a number of M_{cut} values obtained with the cuts in Tabs. 1, 2 and Tab. 6 are presented in Tab. 7. In brackets the results for the $\mathcal{O}(\alpha_{EM}^6)$ contribution alone is also given for the same set of cuts. The corresponding distribution of the mass of the charged lepton, (reconstructed) neutrino and the two most central jets is shown on the left hand side of Fig. 11 for a Higgs mass of 200 GeV (on the left) and for the no Higgs case (on the right). Comparing the results in Tab. 7 with those in Tab. 5 shows

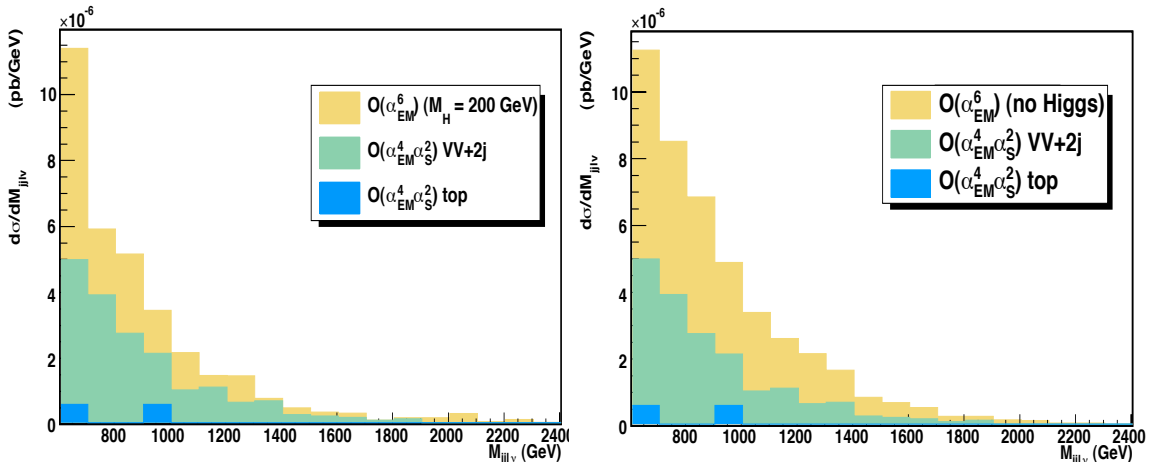


Figure 11: Invariant mass distribution of the two leptons and the two most central jets in the Standard Model with a light Higgs (on the left) and in the no-Higgs scenario (on the right). The cuts applied are listed in Tabs. 1, 2 and Tab. 6. $\mathcal{O}(\alpha_{EM}^6)$ (EW) and $\mathcal{O}(\alpha_{EM}^4\alpha_S^2)$ (QCD) contributions to the differential cross section have been isolated and are shown separately. The $\mathcal{O}(\alpha_{EM}^4\alpha_S^2)$ contributions are further split into *top background* (in blue) and *VV + 2j* (in green). The numbers refer to the $\mu\nu + 4j$ channel only.

that, even with the inclusion of the $\mathcal{O}(\alpha_{EM}^4\alpha_S^2)$ background which contributes equally to the two scenarios, we have been able to maintain a good ratio between the expected number of events in the two cases. If one takes into account only the EW processes the ratio has actually improved. The number of excess events in the no Higgs case has remained almost constant, particularly at large M_{cut} . The additional cuts in Tab. 6 lead to a reduction of the number of signal events by about 45% at $M_{cut} = 600$ GeV and by about 15% at $M_{cut} = 1000$ GeV in the no Higgs case. For a light Higgs the reduction is slightly larger. Fig. 11 shows that the top-related background has been reduced to a negligible level and that the bulk of the background is now given by *VV + 2j* production.

6. Full analysis

In this section we finally analyze all contributions to $\ell\nu + 4j$ simultaneously, building on the experience gained from the study of partial samples in Sect. 4 and 5. In the following we will concentrate on the large invariant mass region for the VV pair $M_{j_c j_c \ell^\pm \nu} > 600$ GeV. In this section and the following one we will consider as signal the sum of the $\mathcal{O}(\alpha_{EM}^6) + \mathcal{O}(\alpha_{EM}^4\alpha_S^2)$ contributions while we refer to the $\mathcal{O}(\alpha_{EM}^2\alpha_S^4)$ processes as background. While this does modify the standard statistical significance, S/\sqrt{B} , which will turn out to be rather large, it does not affect the more refined treatment in terms of confidence levels that we are going to discuss shortly.

We disregard in the following all effects of the interference among the different perturbative orders. The interference between the $\mathcal{O}(\alpha_{EM}^6)$ and $\mathcal{O}(\alpha_{EM}^4\alpha_S^2)$ contributions has been examined for typical generation cuts and found to be of the order of $1 \div 2\%$ compared to

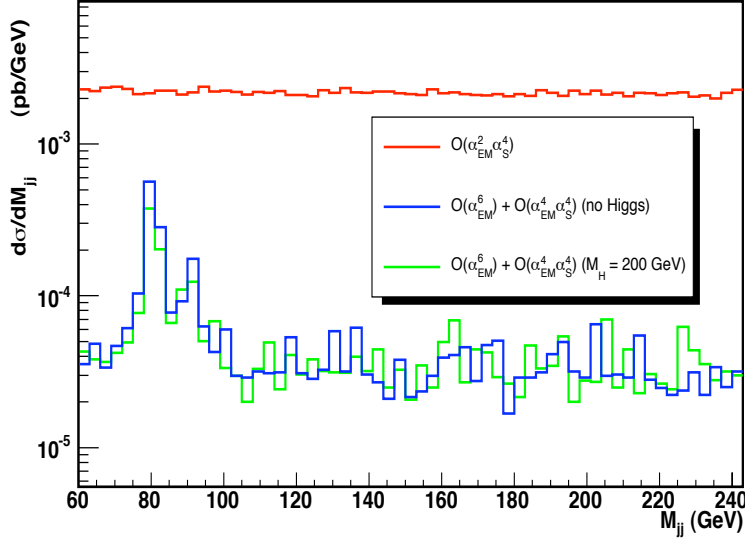


Figure 12: Distribution of the invariant mass of the most central jets. Cuts as in Tabs. 1, 2 and Tab. 6, with the exclusion of the constraint $70 \text{ GeV} < M_{j_c j_c} < 100 \text{ GeV}$, in the mass region $M_{j_c j_c \ell^\pm \nu} > 600 \text{ GeV}$.

M_{cut}	no Higgs		$M_H = 200 \text{ GeV}$		ratio
	σ	events	σ	events	
600 GeV	71.581 fb	7158	70.551 fb	7055	1.01
800 GeV	42.303 fb	4230	41.482 fb	4148	1.02
1000 GeV	25.359 fb	2536	24.886 fb	2489	1.02
1200 GeV	15.817 fb	1582	15.566 fb	1557	1.02
1400 GeV	9.982 fb	998	9.895 fb	990	1.01
1600 GeV	6.506 fb	651	6.489 fb	649	1.00

Table 8: Integrated $\mathcal{O}(\alpha_{EM}^6) + \mathcal{O}(\alpha_{EM}^4 \alpha_S^2) + \mathcal{O}(\alpha_{EM}^2 \alpha_S^4)$ cross section for $M(j_c j_c \ell \nu) > M_{cut}$ and number of expected events after one year at high luminosity ($\mathcal{L} = 100 \text{ fb}^{-1}$) with the set of cuts listed in Tabs. 1, 2 and Tab. 6 in the mass region $M_{j_c j_c \ell^\pm \nu} > 600 \text{ GeV}$ and $70 \text{ GeV} < M(j_c j_c) < 100 \text{ GeV}$. Interferences between the different perturbative orders are neglected. The numbers refer to the $\mu\nu + 4j$ channel only.

the sum of the two contributions. The interference between these two perturbative orders with the $\mathcal{O}(\alpha_{EM}^2 \alpha_S^4)$ term has not been studied but it is expected to be at most of the order of the percent with respect to the non double resonant background, since most of the contributions at $\mathcal{O}(\alpha_{EM}^2 \alpha_S^4)$ do not have a corresponding term in the other orders with the same external particles and color configuration.

In Fig. 12 the invariant mass distribution of the two central jets is shown for the sum of the signal and $VV + 2j$ background in both Higgs scenarios and for the $\mathcal{O}(\alpha_{EM}^2 \alpha_S^4)$ back-

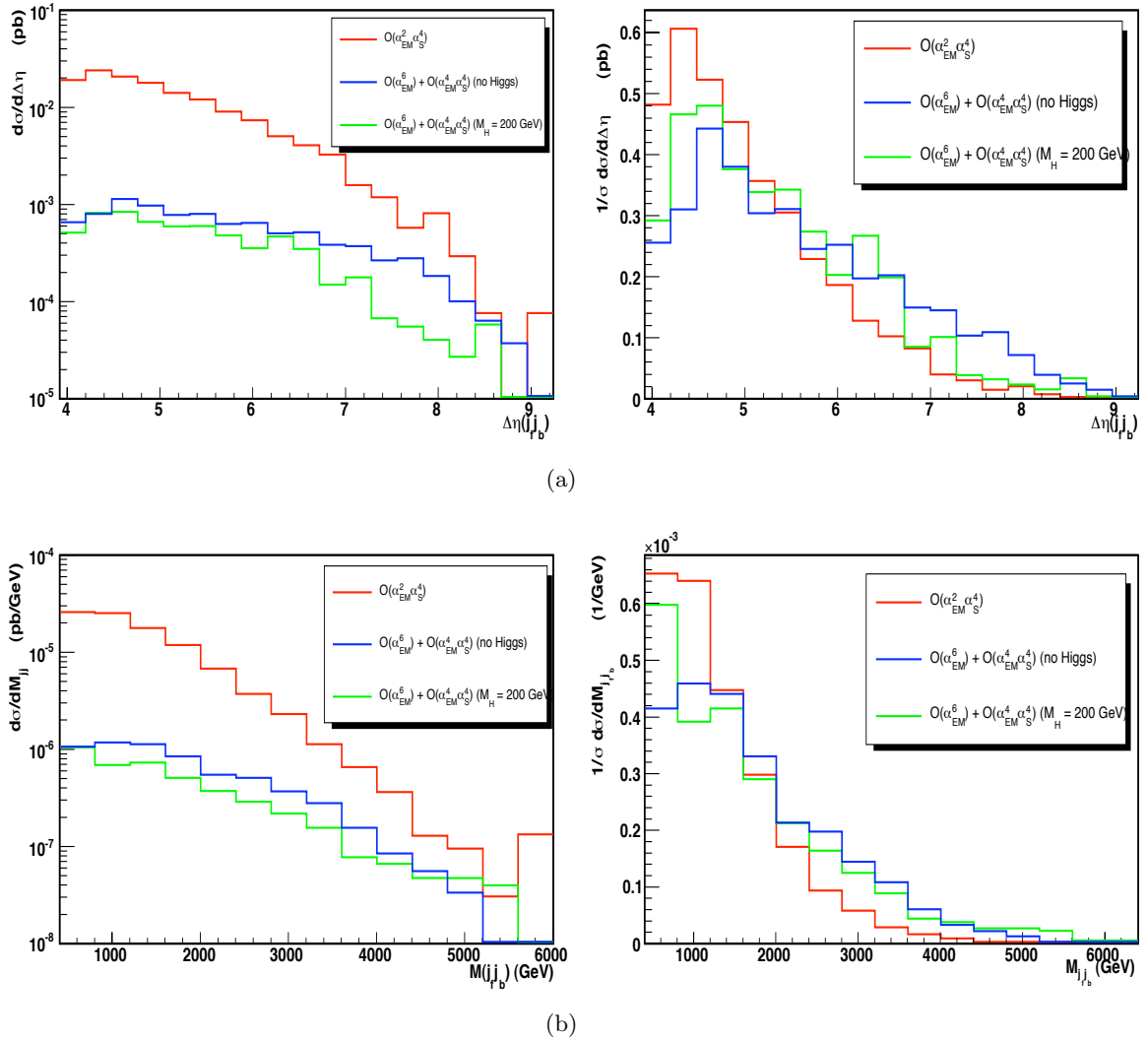


Figure 13: From the top: distribution of the difference in pseudorapidity between tag jets and of the invariant mass of the two tag jets with the cuts of Tabs. 1, 2 and of Tab. 6. The plots on the right are the same as those on the left, but normalized to one. The numbers refer to the $\mu\nu + 4j$ channel only and to the region $M(j_c j_c \nu) > 800\text{GeV}$. Interferences between the two perturbative orders are neglected.

ground. The plot demonstrates that the $\mathcal{O}(\alpha_{EM}^6) + \mathcal{O}(\alpha_{EM}^4 \alpha_S^2)$ contribution is dominated by the production of two electroweak bosons while no particular peak appears around 100 GeV for the $W + 4j$ distribution, as expected.

Fig. 12 clearly shows that the $\mathcal{O}(\alpha_{EM}^2 \alpha_S^4)$ background is much larger than the VV scattering signal, with the present set of selection cuts, even in the neighborhood of the electroweak boson mass peaks and taking into account only large invariant masses for the pair of reconstructed bosons. In order to fully appreciate the degree to which the signal is overwhelmed by the $W + 4j$, the finite resolution in the jet pair invariant mass should be taken into account and signal and background should be compared after integrating over

a reasonable mass window around the vector boson peaks.

The integrated cross section for the sum of all three perturbative orders $M(j_c j_c l \nu) > M_{cut}$ and the number of expected events after one year at high luminosity ($\mathcal{L} = 100 \text{ fb}^{-1}$) for a number of M_{cut} values are shown in Tab. 8. These results have been obtained with the cuts in Tabs. 1, 2 and Tab. 6. In particular they refer to the mass window $70 \text{ GeV} < M_{j_c j_c} < 100 \text{ GeV}$. The excess of events in the no Higgs case is within the statistical uncertainty of the SM prediction.

The last step of the selection procedure is aimed at further enhancing the separation between the two analyzed scenarios while reducing $W + 4j$. Albeit the latter will be subtracted, it is nevertheless fundamental to achieve a good significance of the signal peak since the uncertainty of the background will in the end determine the observability of the signal. In Figure 13 the distributions of the absolute value of the difference in pseudorapidity between tag jets and of the invariant mass of the two tag jets is shown for the different samples. On the right hand side we also present the normalized distributions. It is apparent that the $\mathcal{O}(\alpha_{EM}^2 \alpha_S^4)$ background has typically tag jets with smaller invariant mass and separation in pseudorapidity. In Figure 14 the distributions of the pseudorapidity of the charged lepton, of the missing p_T and of the minimum p_T of the two central jets are shown together with their normalized counterparts. The distributions in Figure 14 clearly show that the vector bosons in the signal sample are usually more central. All the results presented in the two figures are obtained with the cuts of Tabs. 1, 2 and of Tab. 6. Therefore, based on the results of Figure 13 and 14, we apply the cuts in Tab. 9.

Some representative cross sections at high invariant masses are reported in Tab. 10. There are clear indications that the scattering cross section is sensitive to effects of a strongly-coupled gauge dynamics provided the $W + 4j$ background is conveniently subtracted. Indeed, without subtraction, the separation with respect to the Standard Model predictions which has been achieved, of order $\mathcal{O}(15\%)$, would lie within the accuracy of the calculation and, as a result, the underlying sensitivity would be completely spoiled.

Next, as described in Section 2, we proceed with the construction of the discriminator and of its probability density function. In the following we define the background B as the expected yield of the $\mathcal{O}(\alpha_{EM}^2 \alpha_S^4)$ $W + 4j$ processes and the signal S as the expected number of events from all $\mathcal{O}(\alpha_{EM}^6)$ and $\mathcal{O}(\alpha_{EM}^4 \alpha_S^2)$ processes. B and S are random variables representing the number of background and signal events for a possible experimental outcome. \bar{B} and \bar{S} are the corresponding average values which will be taken equal to the predictions of our simulation.

For a reliable estimate of the exclusion limits, two different sources of uncertainty are taken into account. On one side, the number of expected events, both for B and S , is affected by statistical fluctuations. We assume they are distributed according to the Poisson density function,

$$f(N, \bar{N}) = \frac{\bar{N}^N e^{-\bar{N}}}{N!}, \quad (6.1)$$

where \bar{N} is the number of expected events as a consequence of the cross section σ and of the given luminosity \mathcal{L} . On the other hand, the predicted signal cross section is affected

Selection cuts II
$M(j_f j_b) > 1000 \text{ GeV}$
$ \Delta\eta(j_f j_b) > 4.8$
$ \eta(\ell^\pm) < 2.0$
missing $p_T > 100 \text{ GeV}$
$p_T(j_c) > 70 \text{ GeV}$

Table 9: Further selection cuts applied in the final analysis of all samples in addition to the cuts in Tabs. 1, 2 and Tab. 6.

M_{cut}	no Higgs		$M_H = 200 \text{ GeV}$		ratio
	σ	events	σ	events	
600 GeV	6.074 (1.184) fb	607 (118)	5.414 (0.524) fb	541 (52)	1.12 (2.27)
800 GeV	3.758 (0.779) fb	376 (78)	3.288 (0.309) fb	329 (31)	1.14 (2.52)
1.0 TeV	2.255 (0.483) fb	226 (48)	1.941 (0.169) fb	194 (17)	1.16 (2.82)
1.2 TeV	1.317 (0.263) fb	132 (26)	1.148 (0.094) fb	115 (9)	1.15 (2.89)
1.4 TeV	0.683 (0.132) fb	68 (13)	0.601 (0.050) fb	60 (5)	1.13 (2.60)

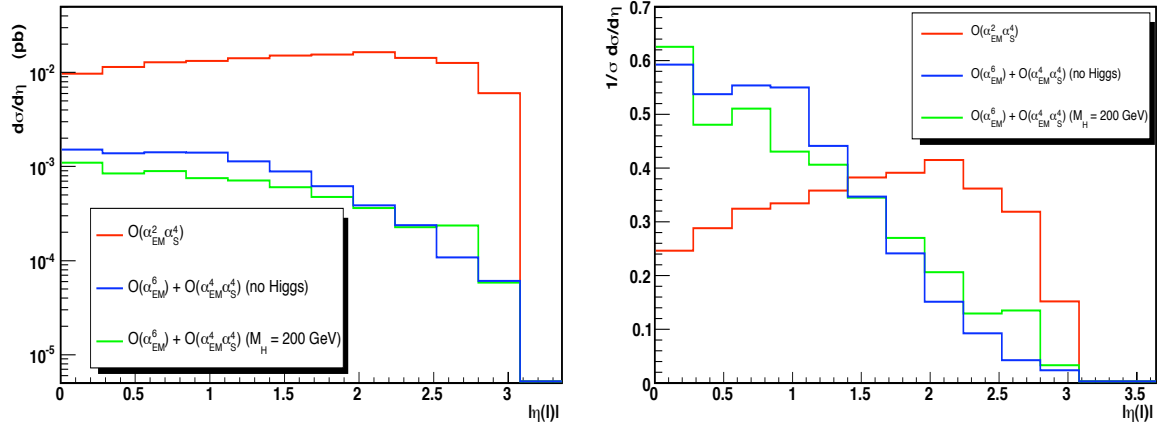
Table 10: Integrated $\mathcal{O}(\alpha_{EM}^6) + \mathcal{O}(\alpha_{EM}^4 \alpha_S^2) + \mathcal{O}(\alpha_{EM}^2 \alpha_S^4)$ cross section for $M(j_c j_c l \nu) > M_{cut}$ and number of expected events after one year at high luminosity ($\mathcal{L} = 100 \text{ fb}^{-1}$) with the set of cuts listed in Tabs. 1, 2 and Tabs. 6, 9. In parentheses the results for the $\mathcal{O}(\alpha_{EM}^6) + \mathcal{O}(\alpha_{EM}^4 \alpha_S^2)$ are also shown. Interferences between the different perturbative orders are neglected. The numbers refer to the $\mu\nu + 4j$ channel only.

by theoretical uncertainties, so the parameter \bar{S} is itself subject to fluctuations. The p.d.f. is eventually calculated as a convolution of the two contributions.

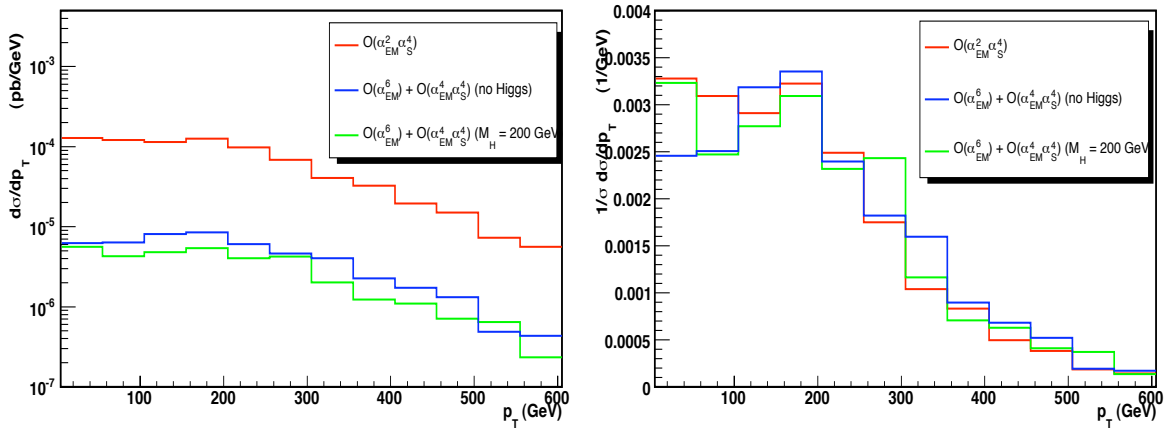
We define the test statistics D using the following prescription,

$$D = B + S - \bar{B} \tag{6.2}$$

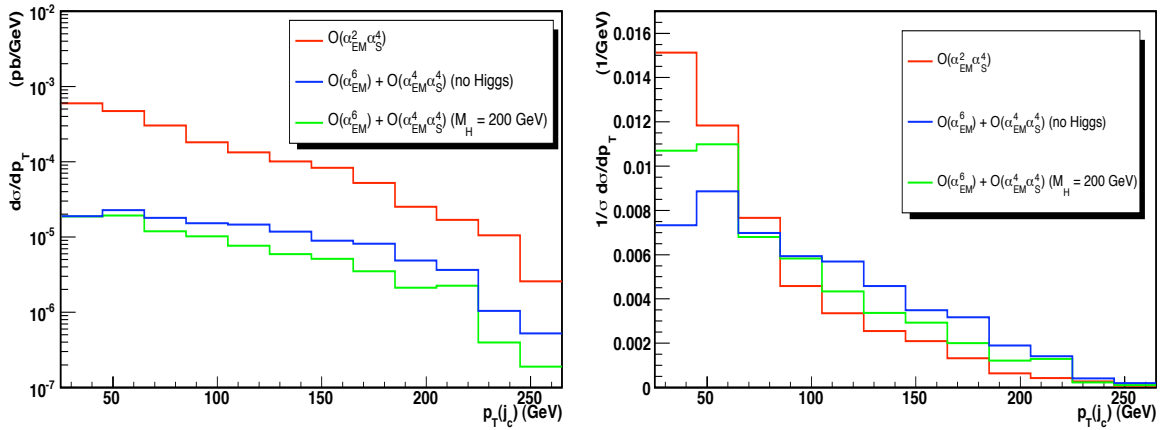
In this analysis, for S we assume, in addition to the statistical fluctuations, a theoretical error defined as a flat distribution in the window $\bar{S} \pm 30\%$ which, in our opinion, is a reasonable choice to account for both pdf's and scale uncertainties for the signal. The processes we are interested in require center of mass energies of the order of the TeV and therefore involve rather large- x quarks, $x \approx 10^{-1} \div 10^{-2}$ at a typical scale Q of about 100 GeV. In this region the uncertainty due to the parton distribution functions is of the order of 5% [40, 41]. As already stated, QCD corrections are in the range of 10% and, as a consequence theoretical uncertainties are expected to be well within this order of magnitude. Only statistical fluctuations have been taken into consideration in the case of B . This is motivated by the fact that the background is likely to be well measured experimentally from the region outside the signal peak, so that the theoretical error on $W + 4j$ is not expected to be an issue at the time when real data analysis will be performed.



(a)

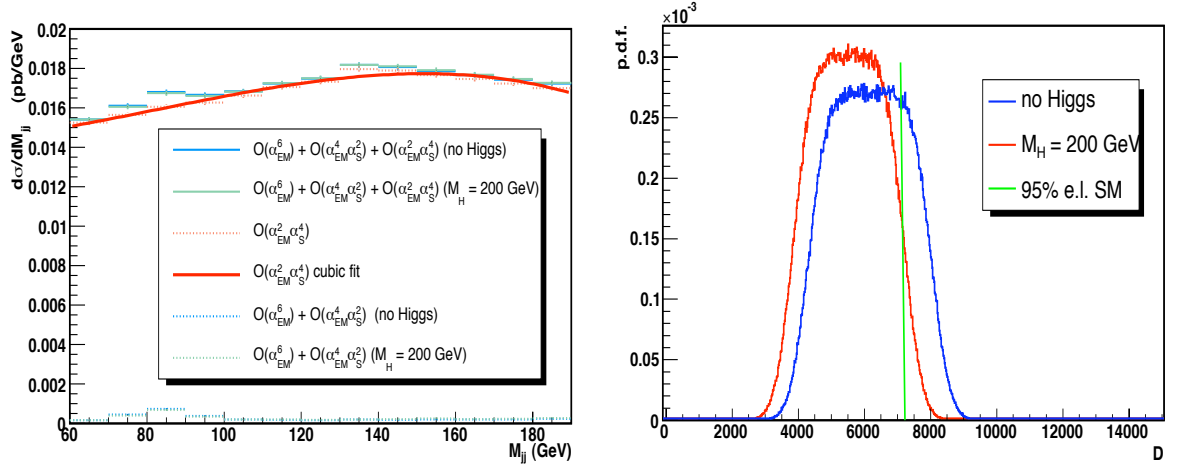


(b)

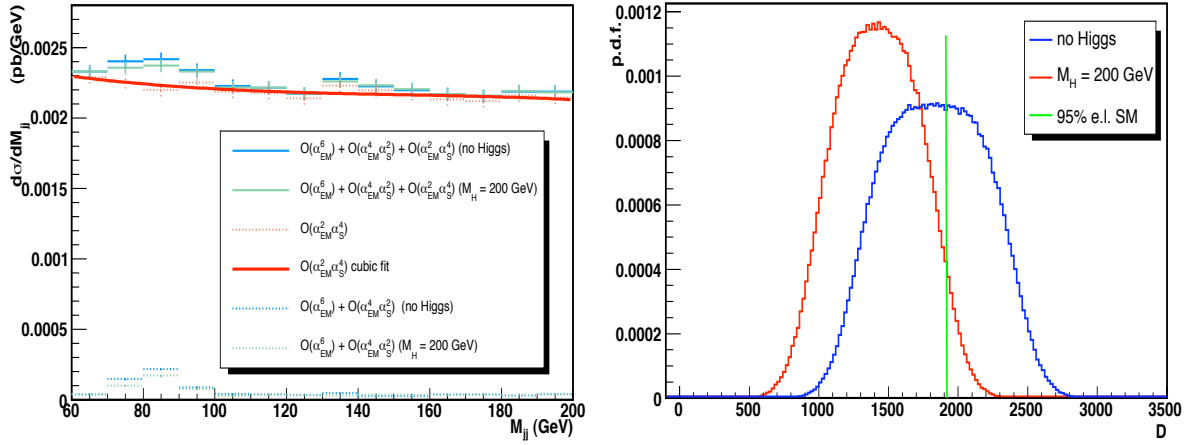


(c)

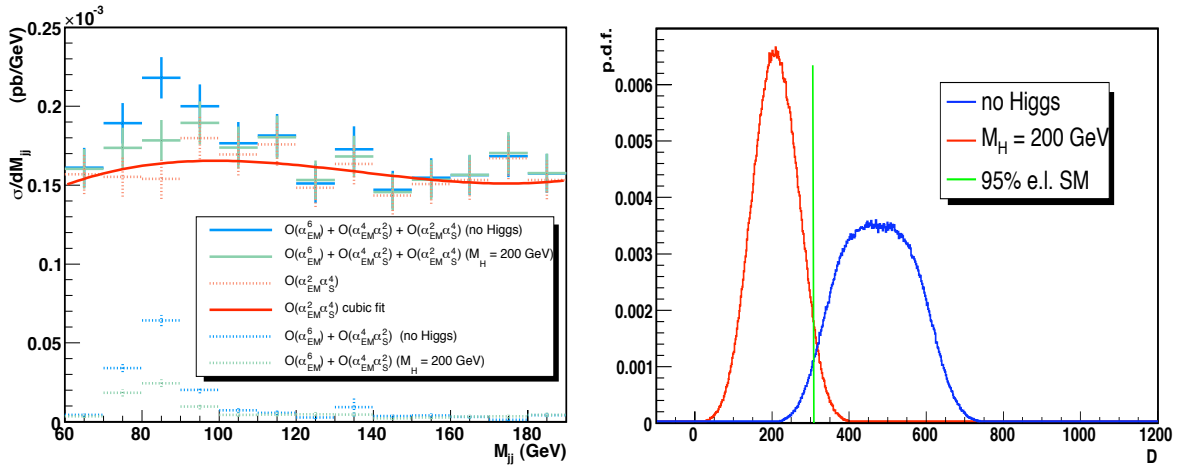
Figure 14: From the top: distribution of the pseudorapidity of the charged lepton, missing p_T and minimum p_T of the two central jets with the cuts of Tabs. 1, 2 and of Tab. 6. The plots on the right are the same as those on the left, but normalized to one. The numbers refer to the $\mu\nu + 4j$ channel only to the region $M(j_c j_c l\nu) > 800\text{ GeV}$. Interferences between the two perturbative orders are neglected.



(a)



(b)



(c)

Figure 15: *On the left:* distribution of the invariant mass of the two central jets: (a) with the cuts of Tabs. 1, 2, (b) with the cuts of Tabs. 1, 2 and Tab. 6, (c) with the full set of cuts Tabs. 1, 2 and Tabs. 6, 9. *On the right:* corresponding probability density function of the test statistics (Eq. 6.2) for the two analyzed scenarios. The cross sections refer to the muon channel only, while the right hand plots assume an integrated luminosity of $\mathcal{L} = 400 \text{ fb}^{-1}$.

Two parameters which well exemplify the effectiveness of the adopted procedure are the significance $\bar{S}/\sqrt{\bar{B}}$ of the signal peak over the non-resonant background and the probability of what we call, for brevity and with a slight abuse of language, the BSM hypothesis at 95% SM exclusion limit, namely the probability that, in the absence of a Higgs boson, the result of an experimental outcome, at fixed luminosity, has a chance of less than 5% in the Standard Model. The first one is related to the possibility of detecting a clear vector boson scattering signal independently of the model assumed. The second parameter is rather an indicator of the resolving power which can be achieved between the two considered prototypes of weakly-interacting and strongly-interacting scenarios. Figure 15 and Tab. 11 show how the sequence of selection cuts manages to improve the separation and the significance of the signal. The red line in the left hand plots is the result of a cubic fit of the $W + 4j$ background in the interval $60 \text{ GeV} < M_{j_c j_c} < 200 \text{ GeV}$. The two curves in the right hand plots are obtained by randomly generating values for the D parameter in Eq.(6.2) as discussed above. In practice we first compute \bar{S} and \bar{B} , where \bar{S} is the number of events for $\mathcal{O}(\alpha_{EM}^6) + \mathcal{O}(\alpha_{EM}^4 \alpha_S^2)$ processes in the mass window $70 \text{ GeV} < M_{j_c j_c} < 100 \text{ GeV}$ corresponding to the plots on the left hand side of Figure 15 for a luminosity of 400 fb^{-1} . \bar{B} is the corresponding number of events for $\mathcal{O}(\alpha_{EM}^2 \alpha_S^4)$ processes, obtained interpolating, as already mentioned, the sidebands between 60 GeV and 200 GeV for the same luminosity and the same mass interval. Then we generate an \bar{S}' from the probability density:

$$P(\bar{S}') = \frac{1}{0.6 \bar{S}} \theta(\bar{S}' - 0.7\bar{S}) \theta(1.3 \bar{S} - \bar{S}') \quad (6.3)$$

corresponding to the assumed theoretical uncertainty. From \bar{B} and \bar{S}' we generate B and S according to the Poisson distributions $f(B, \bar{B})$ and $f(S, \bar{S}')$ respectively. Finally from B and S we construct D according to Eq.(6.2). The normalized frequency of D for the two scenarios is reported in the right hand side of Figure 15. The red curve refers to a Higgs of 200 GeV while the blue one refers to the no-Higgs case. The green vertical line in the right hand plots marks the 95% confidence limit for the SM predictions.

The right hand side of Figure 15 and 16 refer to a luminosity of $\mathcal{L} = 400 \text{ fb}^{-1}$. This corresponds to the sum of the muon and electron channels, $pp \rightarrow \ell\nu + 4j$ ($\ell = \mu, e$), and to 100 fb^{-1} of data for each of the two LHC general-purpose experiments CMS and ATLAS. The cross sections on the left hand side, on the contrary, refer to the muon channel only.

	$\bar{S}/\sqrt{\bar{B}}@no\text{-Higgs}$	$\bar{S}/\sqrt{\bar{B}}@M_H = 200 \text{ GeV}$	$P_{BSM}@95\%CL$
Tabs. 1, 2	14.07 (7.03)	12.61 (6.30)	22.14% (16.54%)
Tabs. 1, 2, 6	11.20 (5.60)	8.69 (4.34)	43.94% (29.17%)
Tabs. 1, 2, 6 and 9	10.72 (5.36)	4.75 (2.37)	96.78% (78.11%)

Table 11: Significances and BSM probabilities with a luminosity $\mathcal{L} = 400 \text{ fb}^{-1}$ and the set of cuts listed in Tabs. 1, 2 and Tabs. 6, 9 are progressively applied. In parentheses the results for a luminosity of $\mathcal{L} = 100 \text{ fb}^{-1}$ are also shown.

The matching significances and BSM probabilities are shown in Tab. 11. In parentheses the results for a luminosity of $\mathcal{L} = 100 \text{ fb}^{-1}$ are also presented: With $\mathcal{L} = 400 \text{ fb}^{-1}$, with the full set of cuts, Tabs. 1, 2 and Tabs. 6, 9, we find that 209 ± 59 signal events are expected in the light Higgs SM scenario and 474 ± 96 in the no Higgs case. Under the given conditions, a number of signal events of approximately 300 units or more would represent an evidence for new physics beyond a light-intermediate SM Higgs at 95% confidence level for SM. Conversely, the probability for a BSM-like experimental outcome to lie below this threshold is 4%.

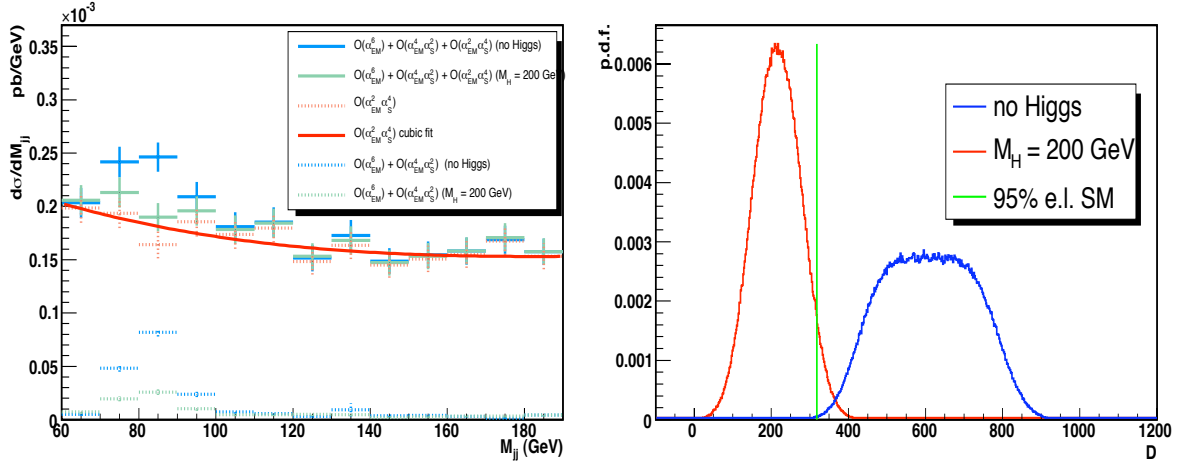
7. Dependence on the jet cone size

Jet resolution is an important experimental issue. At detector level, many analyses make use of the cone algorithm for jet reconstruction which requires hadronic jets to be well separated from each other in the pseudorapidity (η) – azimuthal angle (ϕ) plane within a cone of radius ΔR . The cone algorithm establishes a natural correspondence between jets and the underlying partons. However, due to the large center-of-mass energy available at LHC, some fraction of EW bosons will be highly boosted in the transverse direction and, consequently, the jets from their decays will tend to have a small ΔR separation. Thus, an approach based on the cone separation of jets would eventually result in a severe loss of potentially interesting events: the larger the radius of the cone, the larger the number of discarded events. This could seriously damage the possibility to evidenciate effects of new physics, since the EWSB mechanism is expected to manifest itself in events with very energetic, high- p_T vector bosons.

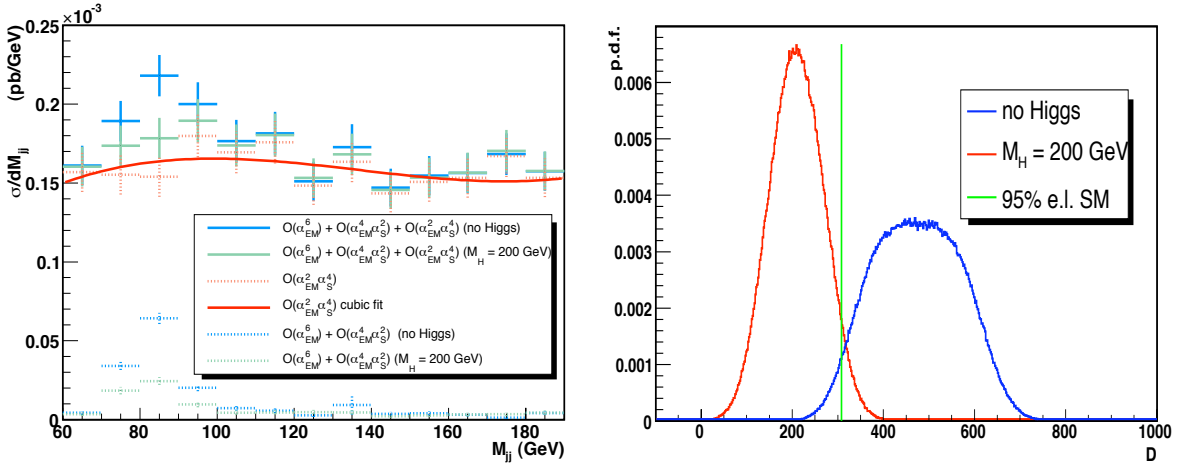
On the other hand, alternative jet finding algorithms have been proposed [42] which may prove useful in connection with this kind of studies as they lead to encouraging results in identifying hadronic decays of heavy bosons via a cut on the sub-jet separation scale.

At the partonic level we are considering, there is no room for addressing the issue of jet resolution in much more detail. The only thing we can do is to investigate what is the impact of requiring a minimum ΔR separation among coloured particles. Of course, the final word is left to a realistic study at the hadronic level, including the full chain of detector simulation and reconstruction.

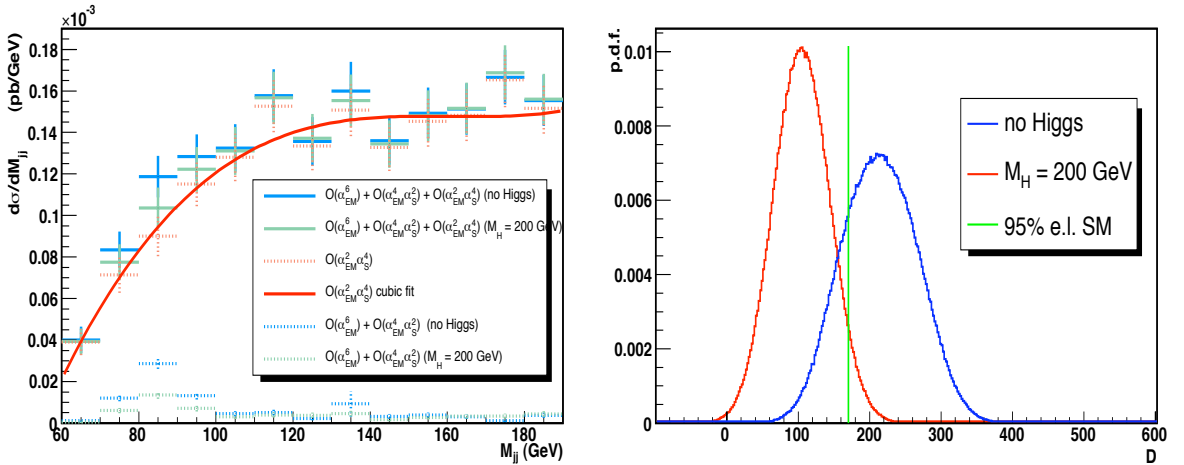
Many experimental analyses adopt a cone size larger than $\Delta R(jj) = 0.3$. It is therefore extremely important to monitor how the final results change with the minimum ΔR imposed for any pair of coloured particles. It should be however mentioned that in all our results we impose a minimum invariant mass of 60 GeV for each pair of coloured particles which partially accounts for jet separation. As shown in Figure 16, the two scenarios tend to align their predictions at larger ΔR thresholds. This effect is related to the fact that, without a Higgs, the outgoing vector bosons are more central and have a larger p_T than in presence of a Higgs boson. As a consequence the probability that the two jets from a boson decay eventually merge into a single jet is higher in the first case. The significances and BSM probabilities corresponding to Figure 16 are shown in Tab. 12. In Figure 17 we show the distribution of the minimum ΔR separation among jets. The results show a rapid decrease of the discriminating power when thresholds above $\Delta R(jj) = 0.5$ are imposed.



(a)



(b)



(c)

Figure 16: Impact of $\Delta R(jj)$ as a criterion for jet separation. *On the left:* distribution of the invariant mass of the two central jets: (a) without any cut on ΔR among coloured particles, (b) with $\Delta R > 0.3$, (c) with $\Delta R > 0.5$. Apart from the ΔR cut, in all cases the full set of cuts in Tabs. 1, 2 and Tabs. 6, 9 is applied. In particular a minimum invariant mass $M(jj) > 60$ GeV has been imposed. *On the right:* corresponding probability density function of the test statistics (Eq. 6.2) for the two analyzed scenarios. The cross sections refer to the muon channel only, while the right hand plots assume an integrated luminosity of $\mathcal{L} = 400 \text{ fb}^{-1}$.

	$\bar{S}/\sqrt{\bar{B}}@no\text{-Higgs}$	$\bar{S}/\sqrt{\bar{B}}@M_H = 200 \text{ GeV}$	$P_{BSM}@95\%CL$
No ΔR	13.05 (6.51)	4.63 (2.31)	99.92% (93.28%)
$\Delta R > 0.3$	10.72 (5.36)	4.75 (2.37)	96.78% (78.11%)
$\Delta R > 0.5$	6.43 (3.24)	3.15 (1.56)	79.91% (48.59%)

Table 12: Significances and BSM probabilities with a luminosity $\mathcal{L} = 400 \text{ fb}^{-1}$ and the set of cuts listed in Tabs. 1, 2 and Tabs. 6, 9 for three values of ΔR separation. In parentheses the results for a luminosity of $\mathcal{L} = 100 \text{ fb}^{-1}$ are also shown.

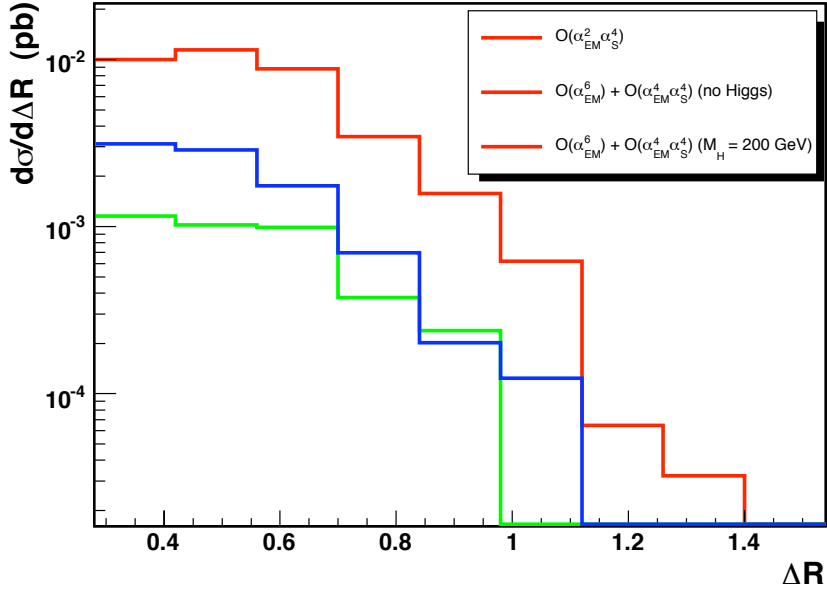


Figure 17: Distribution of the minimum ΔR among all jets with the cuts of Tabs. 1, 2 and of Tabs. 6, 9. The plot refers to the region $M(j_c j_c l \nu) > 600 \text{ GeV}$.

8. Conclusions

We have examined at parton level the process $pp \rightarrow \ell\nu + 4j$ including all irreducible backgrounds contributing to this six parton final state. We have considered two scenarios: a light Higgs Standard Model framework with $M_H = 200 \text{ GeV}$ and an infinite mass Higgs scenario in order to determine whether the two models can be distinguished at the LHC using boson–boson scattering. The largest background is $W + 4j$ which can be subtracted looking at the distribution of the invariant mass of the two most central jets in the region outside the weak boson mass window. We have estimated the probability, in the no Higgs scenario, of finding a result outside the 95% confidence limit in the Standard Model. This probability turns out to be about 97% for an integrated luminosity of $\mathcal{L} = 400 \text{ fb}^{-1}$ and a mass of the reconstructed pair of vector bosons larger than 600 GeV. With the full set

of cuts, Tabs. 1, 2 and Tabs. 6, 9, 209 ± 59 signal events are expected in the light Higgs SM scenario and 474 ± 96 in the no Higgs case. Jet resolution plays a crucial role in the present analysis as in all processes in which high transverse momentum vector bosons or top particles are present and decay hadronically.

Acknowledgments

A.B. wishes to thank the Department of Theoretical Physics of Torino University for support.

This work has been supported by MIUR under contract 2006020509_004 and by the European Community's Marie-Curie Research Training Network under contract MRTN-CT-2006-035505 'Tools and Precision Calculations for Physics Discoveries at Colliders'

References

- [1] Proceedings of the Large Hadron Collider Workshop, Aachen 1990, CERN Report 90-10, G. Jarlskog and D. Rein (eds.).
- [2] A. Djouadi, *The Anatomy of Electro-Weak Symmetry Breaking. Tome I: The Higgs in the Standard Model*, [arXiv:hep-ph/0503172].
- [3] ATLAS Collaboration, *Detector and Physics Performance Technical Design Report*, Vols. 1 and 2, CERN-LHCC-99-14 and CERN-LHCC-99-15.
- [4] K.A. Assamagan, M. Narain, A. Nikitenko, M. Spira, D. Zeppenfeld (conv.) *et al.*, Report of the Higgs Working Group, Proceedings of the Les Houches Workshop on "Physics at TeV Colliders", 2003, [arXiv:hep-ph/0406152].
- [5] CMS Collaboration, *Technical Design Report*, Vols. 1 and 2, CERN/LHCC 2006-001 and CERN/LHCC 2006-021.
- [6] The LEP Collaborations (ALEPH, DELPHI, L3 and OPAL), the LEP Electroweak Working Group and the SLD Heavy Flavour Group, *A combination of preliminary Electroweak measurements and constraints on the Standard Model*, LEPEWWG/2007-01; <http://lepewwg.web.cern.ch/LEPEWWG>.
- [7] The LEP Collaborations (ALEPH, DELPHI, L3 and OPAL), the LEP Electroweak Working Group and the SLD Heavy Flavour Group, <http://lepewwg.web.cern.ch/LEPEWWG>.
- [8] M.S. Chanowitz, *Strong WW scattering at the end of the 90's: theory and experimental prospects*. In *Zuoz 1998, Hidden symmetries and Higgs phenomena* 81-109. [arXiv:hep-ph/9812215]
- [9] T. Appelquist and C.W. Bernard, *Phys. Rev.* **D22** (1980) 200; A.C. Longhitano, *Phys. Rev.* **D22** (1980) 1166; A.C. Longhitano, *Nucl. Phys.* **B188** (1981) 118; T. Appelquist and G.H. Wu, *Phys. Rev.* **D48** (1993) 3235(1993) [hep-ph/9304240].

- [10] J. Bagger, S. Dawson and G. Valencia, *Nucl. Phys.* **B399** (1993) 364; J. Bagger et al., *Phys. Rev.* **D49** (1994) 1246; *Phys. Rev.* **D52** (1995) 3878; A. Dobado, D. Espriu and M. J. Herrero, *Z. Phys.* **C50** (1991) 205; A. Dobado and M. T. Urdiales, *Z. Phys.* **C17** (1996) 965; A. Dobado, M. J. Herrero, E. Ruiz, M. T. Urdiales and R. Pelaez, *Phys. Lett.* **B352** (1995) 400; A. S. Belyaev, O. J. P. Éboli, M. C. Gonzalez-Garcia, J. K. Mizukoshi, S. F. Novaes and I. Zacharov, *Phys. Rev.* **D59** (1999) 015022; O. J. P. Éboli, M. C. Gonzalez-Garcia, and J. K. Mizukoshi, *Phys. Rev.* **D74** (2006) 073005,[arXiv:hep-ph/0606118].
- [11] J. Bagger *et al.*, *Phys. Rev.* **D52** (1995) 3878; A. Dobado, M.J. Herrero, J.R. Peláez and E. Ruiz Morales, *Phys. Rev.* **D62** (2000) 055011,[arXiv:hep-ph/9912224]; J.M. Butterworth,B.E. Cox and J.R. Forshaw, *Phys. Rev.* **D65** (2002) 96014. [arXiv:hep-ph/0201098]
- [12] M. Fabbrichesi and L. Vecchi, arXiv:0703236 [hep-ph].
- [13] A. Alboteanu, W. Kilian and J. Reuter, arXiv:0806.4145 [hep-ph].
- [14] G.F. Giudice, arXiv:0710.3294 [hep-ph].
- [15] D. B. Kaplan and H. Georgi, *Phys. Lett. B* **136** (1984) 183.
- [16] N. Arkani-Hamed, A. G. Cohen and H. Georgi, *Phys. Lett. B* **513** (2001) 232.
- [17] N. S. Manton, *Nucl. Phys. B* **158** (1979) 141; Y. Hosotani, *Annals Phys.* **190** (1989) 233.
- [18] C. Csaki, C. Grojean and H. Murayama, *Phys. Rev. D* **67** (2003) 085012; C. A. Scrucca, M. Serone and L. Silvestrini, *Nucl. Phys. B* **669** (2003) 128.
- [19] K. Agashe, R. Contino and A. Pomarol, *Nucl. Phys. B* **719** (2005) 165.
- [20] R. Contino, T. Kramer, M. Son and R. Sundrum, *JHEP* **0705** (2007) 074.
- [21] G.F. Giudice, C. Grojean, A. Pomarol, R. Rattazzi, [arXiv:hep-ph/0703164].
- [22] R. Barbieri, B. Bellazzini, V.S. Rychkov, A. Varagnolo, arXiv:0706.0432 [hep-ph].
- [23] M.J. Duncan, G.L. Kane and W.W. Repko, *Nucl. Phys.* **B272** (1986) 517; D.A. Dicus and R. Vega, *Phys. Rev. Lett.* **57** (1986) 1110; J.F. Gunion, J. Kalinowski and A. Tofighi–Niaki, *Phys. Rev. Lett.* **57** (1986) 2351.
- [24] R.N. Cahn, S.D. Ellis, R. Kleiss and W.J. Stirling, *Phys. Rev. D* **35** (1987) 1626; V. Barger, T. Han and R. Phillips, *Phys. Rev. D* **37** (1988) 2005 and **D36** (1987) 295; R. Kleiss and J. Stirling, *Phys. Lett.* **200B** (1988) 193; V. Barger *et al.*, *Phys. Rev. D* **42** (1990) 3052; *ibid.* *Phys. Rev. D* **44** (1991) 1426; *ibid.* *Phys. Rev. D* **46** (1992) 2028; D. Froideveaux, in Ref. [1] Vol II, p. 444; M. H. Seymour, *ibid.*, p. 557; U. Baur and E.W.N. Glover, *Phys. Lett.* **B252** (1990) 683; D. Dicus, J. Gunion and R. Vega, *Phys. Lett.* **B258** (1991) 475; D. Dicus, J. Gunion, L. Orr and R. Vega, *Nucl. Phys.* **B377** (1991) 31; J. Bagger *et al.*, *Phys. Rev.* **D49** (1994) 1246; V. Barger, R. Phillips and D. Zeppenfeld, *Phys. Lett.* **B346** (1995) 106; J. Bagger *et al.*, *Phys. Rev.* **D52** (1995) 3878; K. Iordanidis and D. Zeppenfeld, *Phys. Rev.* **D57** (1998) 3072; R. Rainwater and D. Zeppenfeld, *Phys. Rev.* **D60** (1999) 113004; erratum *ibid* **D61** (2000) 099901.
- [25] M.S. Chanowitz and M.K. Gaillard, *Nucl. Phys.* **B261** (1985) 379. M.S. Chanowitz and M.K. Gaillard, *Phys. Lett.* **142B**, 85 (1984) and ref. 1; G. Kane, W. Repko, B. Rolnick, *Phys. Lett.* **B148**, 367 (1984); S. Dawson, *Nucl. Phys.* **B29** (1985) 42.
- [26] E. Accomando, A. Ballestrero, S. Bolognesi, E. Maina and C. Mariotti, *JHEP* **0603** (2006) 093 [arXiv:hep-ph/0512219].

- [27] E. Accomando, A. Ballestrero, A. Belhouari and E. Maina, *Phys. Rev. D* **75** (2007) 113006 [arXiv:hep-ph/0603167].
- [28] G. Bevilacqua, to appear in F. Ambrogini *et al.*, *Proceedings of the Workshop on Monte Carlo's, Physics and Simulations at the LHC PART II*, Frascati, Italy.
- [29] B. Jäger, C. Oleari and D. Zeppenfeld, *JHEP* **0607** (2006) 015, [hep-ph/0603177]; B. Jäger, C. Oleari and D. Zeppenfeld, *Phys.Rev.D*73:113006,2006, [hep-ph/0604200]; G. Bozzi, B. Jäger, C. Oleari and D. Zeppenfeld, *Phys.Rev.D*75:073004,2007, [hep-ph/0701105].
- [30] K. Arnold *et al.*, arXiv:0811.4559 [hep-ph].
- [31] R. Barate *et al.* [LEP Working Group for Higgs boson searches and ALEPH, DELPHI, L3 and OPAL Collaborations], *Phys. Lett. B* **565** (2003) 61 [arXiv:hep-ex/0306033].
- [32] E. Accomando, A. Ballestrero, E. Maina, *JHEP* **0507** (2005) 016, [arXiv:hep-ph/0504009].
- [33] A. Ballestrero, A. Belhouari, G. Bevilacqua, V. Kashkan and E. Maina, *Comp. Phys. Commun.* **180** (2009) 401, arXiv:0801.3359 [hep-ph].
- [34] A. Ballestrero and E. Maina, *Phys. Lett.* **B350** (1995) 225, [arXiv:hep-ph/9403244].
- [35] A. Ballestrero, PHACT 1.0 - *Program for Helicity Amplitudes Calculations with Tau matrices* [arXiv:hep-ph/9911318] in *Proceedings of the 14th International Workshop on High Energy Physics and Quantum Field Theory (QFTHEP 99)*, B.B. Levchenko and V.I. Savrin eds. (SINP MSU Moscow), pg. 303.
- [36] F. Maltoni, T. Stelzer, *JHEP* 0302 (2003) 027; T. Stelzer and W. F. Long, *Comput. Phys. Commun.* **81** (1994) 357;
J. Alwall *et al.*, arXiv:0706.2334;
H. Murayama, I. Watanabe and K. Hagiwara, KEK-91-11.
- [37] J. Alwall *et al.*, A Standard format for Les Houches event files. Written within the framework of the MC4LHC-06 workshop: Monte Carlos for the LHC: A Workshop on the Tools for LHC Event Simulation (MC4LHC), Geneva, Switzerland, 17-16 Jul 2005, *Comp. Phys. Commun.* **176** (2007) 300, [arXiv:hep-ph/0609017].
- [38] CTEQ Coll.(H.L. Lai *et al.*) *Eur. Phys. J.* **C12** (2000) 375.
- [39] N.Amapane *et al.*, CMS Note AN-2007/05.
- [40] A.D. Martin, R.G. Roberts, W.J. Stirling and R.S. Thorne, *Eur. Phys. J.* **C28** (2003) 455, [hep-ph/0211080].
- [41] A.D. Martin, R.G. Roberts, W.J. Stirling and R.S. Thorne, *Eur. Phys. J.* **C35** (2004) 325, [hep-ph/0308087].
- [42] J.M. Butterworth, J. Ellis and A.R. Raklev, *JHEP* **0705** (2007) 033, [arXiv:hep-ph/0702150].